CHARACTERISTICS OF CATIONIC RED X-GRL ADSORPTION BY RAW DIATOMITE AND DIATOMITE CONCENTRATE

Zijie REN, Junfang GUAN, Huimin GAO, Jingjing TIAN, Yafei WEN, Renji ZHENG

School of Resources and Environment Engineering, Wuhan University of Technology, Wuhan 430070, China, guanjfang@163.com

Abstract: Raw diatomite (RD) and diatomite concentrate (DC) were used for the adsorption of cationic Red X-GRL from aqueous solutions. Mono-factor experiments were carried out to investigate the effects of the operation factor, and adsorption kinetics, isotherms, thermodynamics and mechanisms were explored. Similar trend for X-GRL adsorption onto RD and DC was observed. The adsorption capacity of dyes increased slightly with temperature, and the neutral pH was the optimum level. The adsorption processes occurred in accordance with the pseudo second-order model and were well fitted by the Langmuir isotherm model. The main driving forces of the physical adsorption on the diatomite were electrostatic attraction and van der Waals force. The RD could uptake more X-GRL than DC due to its higher content of fine particle and therefore, due to higher surface area available for adsorption. Raw diatomite as a cheap absorbent for X-GRL removal can be suggested as a promising supplement to activated carbon.

Keywords: diatomite, dye, adsorption, fine particles

Introduction

Dyes, which form a class of colored chemicals, have been used in textile, leather, paper, plastic, and other industries for a long time (Yu and Fugetsu, 2010). If discharged without any treatment, the dyes are not only toxic to aquatic life, but are also potentially carcinogenic that can cause severe damage to human beings (Bea and Freeman, 2007; Lei et al., 2007; Amin, 2009). More than 60% of the global commercial dyes are Azo dyes (Isil and Sponza, 2005). The cationic Red X-GRL (X-GRL) is a very popular azo dye and widely used in dying acrylic and blended fabric (Qiu et al., 2012). Physical adsorption, because of its low cost, high efficiency, easy handling, wide variety of adsorbents, and high stabilities towards the adsorbents, has become the mostly widely used method for eliminating dyes (Yu and Fugetsu, 2010; Wu et al., 2008; Lin et al.,

2007). The active carbon is the most common and effective absorbent, but its use is limited due to a costly regeneration process (Lim and Okada, 2005).

Diatomite is a non-metallic mineral raw material, which is composed of skeletal remains of single-cell water plants (algae). Diatomite is approximately 500 times cheaper than commercial activated carbon (Erdem et al., 2005). Because of its complex structure with abundant fine microscopic pores, cavities and channels, diatomite has long been applied as a filter aid, filler, insulator, and catalyst support (Ediz et al., 2010; Wang et al., 2011; Bahramian et al., 2008). The diatomite also can eliminate water-soluble organic dyes, especially cationic dyes, because of the silanol groups available on the surface of diatomite particles (Khraisheh et al., 2005A). Diatomite or modified diatomite has shown its effectiveness for the removal of methylene blue, reactive black, reactive yellow (Khraisheh et al., 2005A,B; Tsai et al., 2004), telon red A2R and ramazol golden yellow RGB (Lin et al., 2007), but its use for the removal of X-GRL has not been mentioned previously.

China has substantial diatomite resources, most of which are of moderate quality, having a SiO_2 content of about 60%-80% (Sun et al., 2013). The impurities in the raw diatomite may block the pores in the diatom skeletons, and thereby decrease the adsorption ability. A comparative study of the adsorption of X-GRL onto low grade diatomite (RD) and diatomite concentrate (DC) obtained by purifying low grade diatomite has not been conducted before.

Objective of this study is to investigate the effects of main operational parameters aiming X-GRL removal by raw diatomite (RD) and diatomite concentrate (DC). Kinetic model, equilibrium isotherm and some thermodynamic parameters were estimated from experimental results. Further, the mechanism of adsorption was explored.

Materials and methods

Materials

The low grade diatomite (RD) was obtained from the Linjiang region of China. The diatomite concentrate (DC) used for the adsorption tests was obtained by scrubbing technique and centrifugation of RD using the previously described procedures (Sun et al., 2013). The chemical and phase compositions of RD and DC were determined by an X-ray Fluorescence (XRF, Axios advanced, PAN Alytical B.V., Netherlands) and X-ray Diffractometer (XRD, D/Max-IIIA, RIGAKU, Japan) with monochromatic Cu K α radiation in 5–70° at a rate of 0.02°/s. The results of XRF and XRD are shown in Table 1 and Fig. 1, respectively.

DC had higher SiO_2 content and lower extents of Al_2O_3, Fe_2O_3, K_2O than the RD. The phase analysis showed that the amorphous opal was the main component, and small amount of illite, quartz and plagioclase existed in both the RD and DC (Ren et al., 2014). However, the extent of impurities in DC was lower than those in RD. The chemical structure of cationic Red X-GRL, the azo-dye used for the adsorption tests with DC and RD, is presented in Fig. 2 (Lei et al., 2007; He et al., 2009; Li et al., 2010).

Table 1. Chemical composition of RD and DC

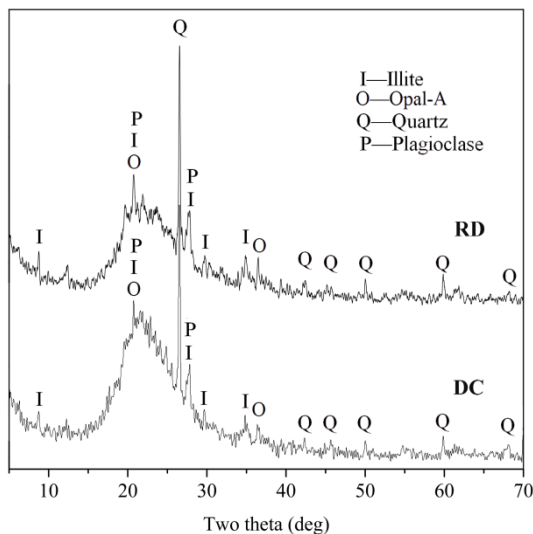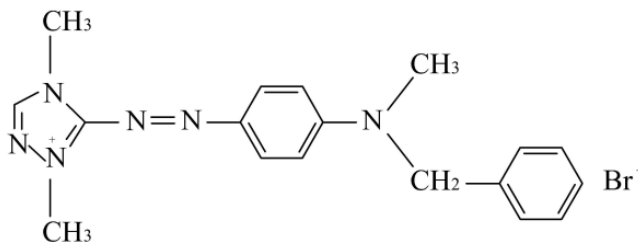| Component	SiO_2	Al_2O_3	Fe_2O_3	CaO	K_2O	Na_2O	L.O.I.[a]
RD (wt. %)	78.37	7.15	4.45	0.46	1.00	0.40	6.46
DC (wt. %)	85.54	3.78	1.81	0.40	0.76	0.47	6.41

[a] Loss on ignition

Fig. 1. XRD patterns of RD and DC

Fig. 2. Chemical structure of cationic Red X-GRL

Adsorption tests

The diatomite sample was added into 50 cm^3 X-GRL aqueous solution with particular concentration. The solution was agitated at 150 rpm in a thermostat shaker (85-2, Wenhua, Jintan, China) prior to centrifuging at 4000 rpm for 5min. The supernatant was used to determine the concentration of the residual X-GRL using a MAPADA, V-1100D spectrophotometer at 535nm. The conditions of adsorption experiments are given in Table 2. The final concentrations were calculated with the absorbance

standards curve. The X-GRL removal data was calculated using the method described by Lei et al. (2007).

Table 2. Conditions of adsorption experiments

	Adsorption temp. (°C)	pH	Initial Con. of X-GRL (mg/dm^3)	Adsorbent Con. (g/dm^3)	Contact time (min)
Effect of adsorption temp.	20–40	7	20	0.8	0.5–15
Effect of adsorbent con.	20	7	20	0.6–2.4	5
Effect of initial pH	20	3–11	20	0.8	9
Effect of initial con. of X-GRL	20	7	4–28	0.8	5

Analytical methods

The morphology of the diatomite skeletons in RD and DC was identified by scanning electron microscopy (SEM, JSM-5610LV, JEOL Ltd., Japan) with an accelerating voltage of 20 kV. Adsorbent samples were removed from the X-GRL solution after equilibrium is achieved and drying at 70 ℃ for preparation for the analysis. FT-IR spectra of the samples were obtained using a Nicolet spectrophotometer (IS-10, US).

Results and discussion

Effect of operation parameters

The mono-factor experiment method was adopted to investigate the effect of individual operational parameters including temperature, adsorbent concentration, initial pH, and initial concentration of X-GRL. Figure 3 shows the influence of these parameters on X-GRL removal.

Effect of adsorption temperature

As shown in Fig. 3a, the adsorption of X-GRL onto RD increased rapidly with increasing contact time from 0 to 1 min. The fast adsorption at the initial stage may be due to the higher driving force along with the availability of both the uncovered surface area and the active silanol groups on the RD. Subsequently, the adsorption rate slowed down with further increase in contact time. This could be attributed to the reduction of both the extent of the uncovered surface area and remaining active silanol groups. It took around 11 minutes to reach adsorption equilibrium for X-GRL on to RD.

The adsorption of X-GRL onto DC also increased with an increase in contact time, but at a comparatively slower rate as compared to adsorption onto RD (Fig. 3b). It also took around 11 minutes to reach adsorption equilibrium for X-GRL onto DC, while the X-GRL removal rate by DC was much lower. An increase in the X-GRL uptake onto both the RD and DC was observed with an increase in temperature from 20 to 40 ℃. This indicates that X-GRL adsorption on both the RD and DC was an endothermic process.
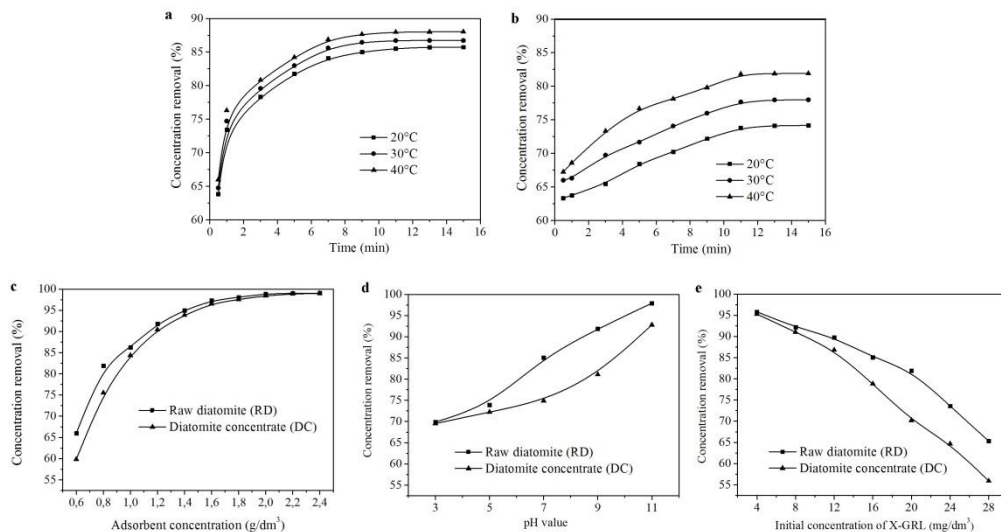
Fig. 3. X-GRL removal with respect to; (a) temperature for RD, (b) temperature for DC,
(c) adsorbent concentration, (d) initial pH, (e) initial X-GRL concentration

Effect of adsorbent concentration

The influence of adsorbent concentration on X-GRL removal is shown in Fig. 3c. As the RD and/or DC concentration increased from 0.6 to 2.4 g/dm^3, the X-GRL removal rate increased from around 60% up to 100%. When the adsorbent concentration was lower than 1.4 g/dm^3, the X-GRL removal rates by RD were higher than those by DC. However, the difference in removal rate decreased gradually after 1.4 g/dm^3, and the X-GRL removal rate reached 99% at 2.4 g/dm^3. Obviously, the higher the amount of diatomite disposed into the aqueous solution, the higher was the X-GRL absorption.

Effect of initial pH

Figure 3d shows notable increases in the X-GRL adsorption by RD and DC in a pH range of 3–11. However, the degradation of X-GRL by OH^- was very obvious. Before adding any adsorbent, the X-GRL removal rate reached to over 80% in the pH of 9–11. In a previous work it has been proved that the auxochrome of some kinds of dyes may be affected from the absence of OH^- in alkaline conditions (Hao et al., 2000). The reason for the low removal rates in acid conditions is the fact that excess H^+ ions compete with the dye cation to adsorb onto available sites on the adsorbent surface. In this regard, the neutral pH is the optimum condition for the X-GRL removal onto RD and DC.

Effect of initial concentration of X-GRL

As shown in Fig. 3e, with the increase of initial concentration of X-GRL from 4 to 28 mg/dm^3, the rate of adsorption of X-GRL on both RD and DC significantly decreased. This can be attributed to the fact that higher initial concentration of X-GRL corresponds

to a higher extent of X-GRL molecules, and the removal rate will therefore be lower as the amount of adsorbent remains unchanged.

Adsorption kinetics, isotherms and thermodynamics

Adsorption kinetics

Two kinetic models, namely, pseudo-first-order and pseudo-second-order are analyzed according to the method reported by Ho and McKay (1999) and Ho et al. (2000). From the slope and intercept of straight portion of the linear plots obtained by plotting ln (q_e-q) vs. t (Fig. 4a), the values of the pseudo-first-order rate constants k_1 and q_e were calculated and listed in Table 3. Figure 4b shows the plot of t/q_t against t. The values of the pseudo-second-order rate constants k_2 and q_e (Table 3) were determined from the slope and intercept of the plot.
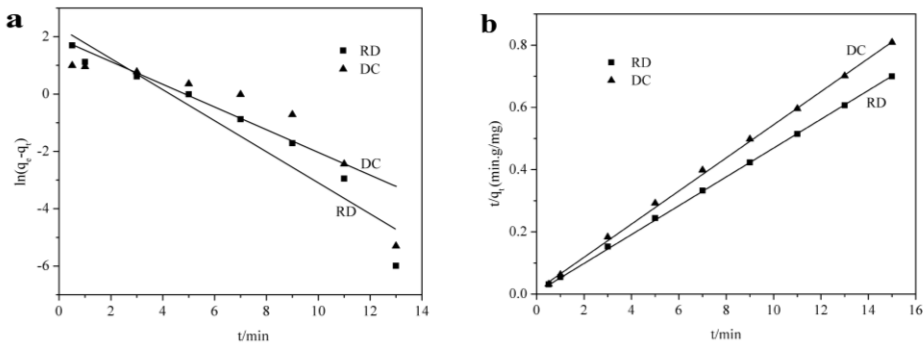

Fig. 4. Comparison of kinetics of X-GRL adsorption onto RD and DC according to
(a) pseudo-first-order, (b) pseudo-second-order

Table 3. Kinetic parameters for X-GRL adsorption by RD and DC

	equation	sample	model	parameters		
				k_1	q_e	R^2
Pseudo 1st order model	$\ln(q_e - q_t) = Lnq_e - k_1t$	RD	$\ln(q_e - q_t) = -0.523t + 2.225$	0.523	9.25	0.915
		DC	$\ln(q_e - q_t) = -0.425t+1.960$	0.425	7.10	0.803
				k_2	q_e	R^2
Pseudo 2nd order model	$\dfrac{t}{q_t} = \dfrac{1}{k_2 q_e^{2}} + \dfrac{1}{q_e}t$	RD	$t/q_t = 0.046t + 0.011$	0.192	21.74	0.999
		DC	$t/q_t = 0.053t + 0.017$	0.165	18.87	0.999

The results show that both of the correlation coefficients of the pseudo-second-order model for RD and DC are 0.999, and these values are larger than those obtained according to the pseudo-first-order model (0.915 and 0.803). This implied that the adsorption of X-GRL onto RD and DC was better represented the pseudo-second-order model.

Equilibrium isotherms

The equilibrium data were analyzed according to two isotherm equilibrium models, namely, Langmuir and Freundlich. Parameters were obtained using the method described previously (He et al., 2009; Li et al., 2011). From the slope and intercept of straight portion of the linear plots of C_e/q_e vs. C_e (Fig. 5a), the parameters of the Langmuir equations were calculated and listed in Table 4. Figure 5b shows the plot of $\ln q_e$ against $\ln C_e$. The parameters of the Freundlich equations (Table 4) were determined from the slope and intercept of the plot.
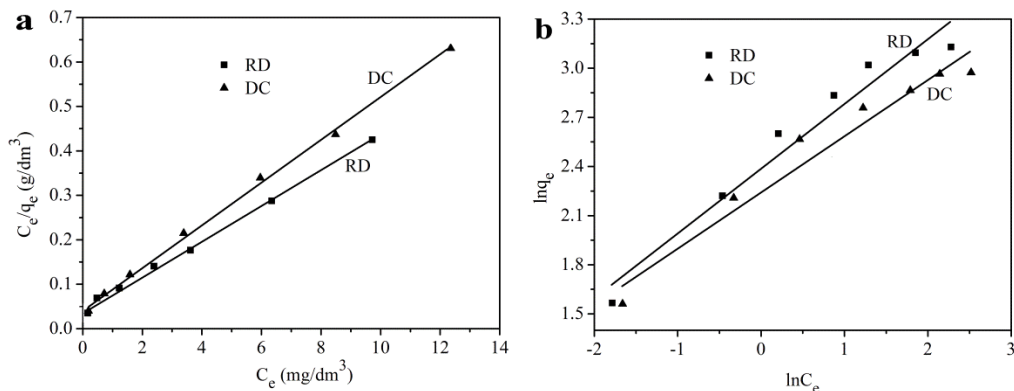

Fig .5. Isotherm equilibrium models of X-GRL adsorption onto RD and DC
according to Langmuir (a), Freundlich (b)

The Langmuir isotherms represented the X-GRL adsorption onto RD and DC in a better way as has been indicated by the comparatively higher R^2. This corresponds to monolayer adsorption behavior of X-GRL onto RD and DC. According to the fitting results, the corresponding monolayer saturated adsorption capacity for RD and DC reaches 25.19 mg/g and 20.96 mg/g, respectively.

Table 4. Parameters of Langmuir and Freundlich equations

Sample	Langmuir			Freundlich		
	q_m (mg/g)	K_L (dm^3/mg)	R^2	K_F (dm^3/mg)	$1/n$	R^2
RD	25.19	1.04	0.998	11.00	0.40	0.959
DC	20.96	1.09	0.998	9.60	0.34	0.955

Thermodynamic study

Due to a better representation of X-GRL adsorption onto RD and DC by the Langmuir isotherms, the thermodynamic data could be calculated using Van't Hoff equations. From the slope and intercept of straight portion of the linear plots of $\ln K_d$ vs. $1/T$ (Fig.6), the values of the standard enthalpy change (ΔH) and standard entropy change (ΔS) were

calculated. The calculated thermodynamic parameters (standard free energy changes (ΔG), standard enthalpy change (ΔH), standard entropy change (ΔS)) at each temperature and equilibrium adsorption amount for RD and DC are presented in Table 5 and Table 6, respectively.
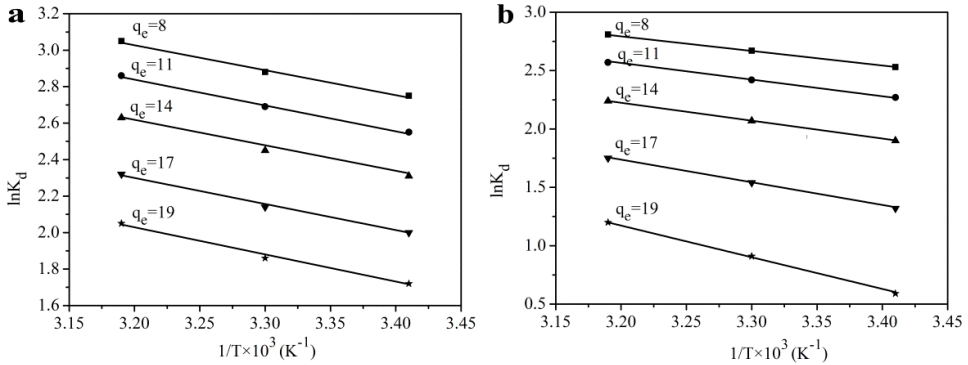

Fig. 6. Fitted curves of changes of standard enthalpy and standard entropy
of X-GRL adsorption on RD (a) and DC (b)

Table 5. Values of thermodynamic parameters for absorption of X-GRL
onto RD with respect to temperature and equilibrium adsorption amount

q_e (mg/g)	ΔH (KJ/mol)	ΔS J/(mol·K)	ΔG/(kJ/mol)		
			293K	303K	313K
8.0	11.76	62.91	-6.69	-7.26	-7.95
11.0	11.88	61.71	-6.22	-6.78	-7.45
14.0	12.06	60.34	-5.64	-6.18	-6.85
17.0	12.37	58.79	-4.87	-5.39	-6.05
19.0	12.75	57.71	-4.18	-4.69	-5.34

Table 6. Values of various thermodynamic parameters for absorption
of X-GRL onto DC with respect to temperature and equilibrium adsorption amount

q_e/ (mg/g)	ΔH /(KJ/mol)	ΔS /J/(mol·K)	ΔG/(KJ/mol)		
			293K	303K	313K
8.0	10.67	57.45	−6.17	−6.74	−7.32
11.0	11.42	57.83	−5.52	−6.09	−6.68
14.0	12.81	59.54	−4.63	−5.22	−5.82
17.0	16.15	66.15	−3.22	−3.88	−4.55
19.0	23.39	84.72	−1.43	−2.30	−3.12

These results show that there is a similar trend in terms of thermodynamic parameters for RD and DC. The negative values of ΔG at all studied conditions indicate

that the adsorption of X-GRL onto RD and DC followed a spontaneous trend. Besides, physical adsorption could be accepted to have played an important role in the X-GRL uptake by both adsorbents, as confirmed by the ΔG values ranging between -20 to 0 kJ/mol. The positive values of ΔH at all studied conditions revealed that the adsorption was an endothermic process and this was supported by the increasing removal rate with rising temperature. The positive values of ΔS reflected the affinity of X-GRL towards RD and DC, and also indicated increased randomness at the adsorbent/solution interface during adsorption (Li et al., 2011).

Adsorption mechanisms

The FT-IR spectra of X-GRL, RD, DC and the diatomite samples after adsorption are presented in Fig. 7. The band at around 3440 cm^{-1} is due to the stretching vibrations of adsorbed water, and the band at 1635 cm^{-1} reflects H-O-H bending vibration of water. For RD and DC, the bands at around 1097, 797 and 469 cm^{-1} represent the asymmetric stretching, symmetric stretching and bending vibrations of Si-O-Si bonds, respectively (Saidi et al., 2012; Xiao et al., 2004). Compared with RD, the SiO$_2$ content of DC was higher as shown by the relatively higher intensity of the peak at 1097 cm^{-1}, which complies with the results of the XRF and XRD analysis. Moreover, the intensity of the bands at 3435 and 1097 cm^{-1} increased when the dye was adsorbed onto RD and DC. These two bands also tended to occur at higher wavenumbers after adsorption under the influence of the 3447 and 1147 cm^{-1} bands of the azo-dye, X-GRL.

Figure 8 shows the morphology of RD and DC obtained by SEM. It is known that the fine particles rejected by concentration consisted of little extents of diatomite skeletons and clay particles. The specific surface area decreased from 27.3 to 13.0 m^2/g after concentration of diatomite. The decrease of specific surface area was attributed to the removal of these fine impurities with relatively higher specific surface areas (Ediz et al., 2010; Sun et al., 2013). It was previously shown that clay minerals like illite with high surface area could have a remarkable ability of dye adsorption (Kahr and Madsen, 1995). In this respect, it could be claimed that RD with a higher content of fine particles and thus, higher surface area could uptake more X-GRL as compared to DC.

It is known that the zero point of charge (ZPC) of diatomite is around pH 5.4. Diatomite surface is degenerated by -OH groups and oxygen bridges, which act as adsorption sites. The reason for the poor removal of X-GRL at lower pH's than the ZPC condition is that the electrostatic repulsion between positively charged X-GRL molecules and the diatomite surface was increased. With a pH higher than the ZPC value, negative charges on the biomass surface starts to accumulate, and cationic X-GRL becomes attractable to the diatomite surface (Khraisheh et al., 2005A; Vijayaraghavan et al., 2008). These findings comply with the findings about the effects of initial pH in this study.

There is an electrostatic attraction between the X-GRL molecules and the negatively charged diatomite surface. The X-GRL is hydrophilic in nature due to the hydration of polar groups and charged groups in the molecular structure of X-GRL (He et al., 2009),

and hence, the X-GRL molecules adsorb onto diatomite surface through van der Waals force. In this respect it could be deduced that the main driving forces of the physical adsorption of the azo-dye, X-GRL on diatomite were electrostatic attraction and Van der Waals force.
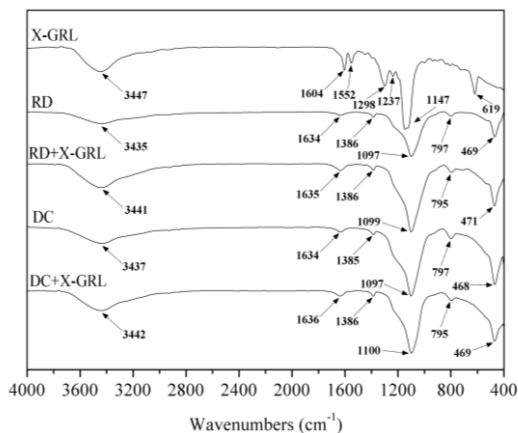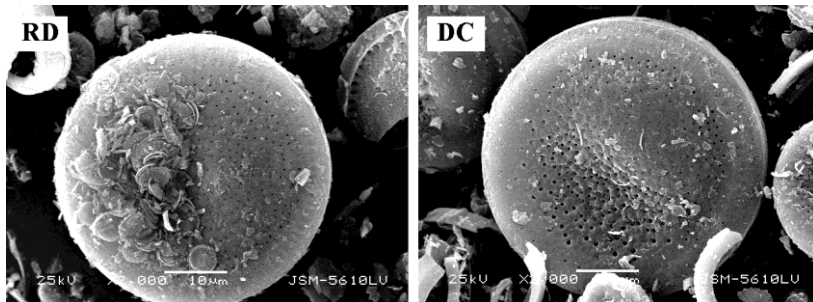

Fig. 7. FT-IR spectra of the samples

Fig. 8. SEM images of RD and DC

Conclusions

Similar mechanisms were found responsible for X-GRL adsorption onto raw diatomite (RD) and diatomite concentrate (DC). The equilibrium adsorption capacity of RD and DC increased slightly with temperature, and the neutral pH condition was found to favour the adsorption process. Adsorption processes was best represented by the pseudo-second-order model, the Langmuir adsorption isotherms. Adsorption was endothermic under all conditions. The adsorptions followed a spontaneous trend, and physical adsorption could have played an important role. The main driving forces of the physical adsorption of X-GRL on the diatomite were electrostatic attraction and Van der

Waals forces. Also, it was seen that RD could uptake more X-GRL than DC owing to higher content of fine particles with higher surface area. In view of the findings of this study, raw diatomite can be suggested as a cost-effective absorbent alternative to active carbon for the removal of azo-dye, X-GRL.

Acknowledgements

References

AMIN N.K., 2009, *Removal of direct blue-106 dye from aqueous solution using new activated carbons developed from pomegranate peel: adsorption equilibrium and kinetics*, J. Hazard. Mater. 165, 52–62.

BAE J. S., FREEMAN H. S., 2007, *Aquatic toxicity evaluation of new direct dyes to the daphnia magna*, Dyes Pigments, 73, 81–85.

BAHRAMIAN B., ARDEJANI F.D., MIRKHANI V., BADII K., 2008, *Diatomite-supported manganese Schiff base: An efficient catalyst for oxidation of hydrocarbons*, Appl. Catal. A: Gen. 345, 97–103.

EDIZ N., BENTLI I., TATAR I., 2010, *Improvement in filtration characteristics of diatomite by calcination*, Int. J. Miner. Process. 94, 129–134.

ERDEM E., COLGECEN G., DONAT R., 2005, *The removal of textile dyes by diatomite earth*, J. Colloid Interface Sci. 282, 314–319.

HAO O.J., KIM H., CHIANG P.C., 2000, *Decolorization of wastewater*, Crit. Rev. Environ. Sci. Technol. 30, 449–505.

HE S.H., ZHOU Y., GU Z.P., XIE S.B., DU X., 2009, *Adsorption of two cationic dyes from aqueous solution onto natural attapulgite*, Int. Conf. Bioinformatics Biomed. Eng., iCBBE. 1–5.

HO Y. S., MCKAY G., 1999, *Pseudo-second order model for sorption processes*, Process. Biochem. 34, 451–465.

HO Y. S., NG J. C. Y., MCKAY G., 2000, *Kinetics of pollutant sorption by biosorbents: Review*, Sep. Purif. Methods. 29, 189–232.

ISIL M., SPONZA D.T., 2005, *Effects of alkalinity and co-substrate on the performance of an upflow anaerobic sludge blanket (UASB) reactor through decolorization of Congo Red azo dye*, Bioresour. Technol. 96, 633–643.

KAHR G., MADSEN F.T., 1995, *Determination of the cation exchange capacity and the surface area of bentonite, illite and kaolinite by methylene blue adsorption*, Appl. Clay Sci. 9, 327–336.

KHRAISHEH M.A.M. , AL-GHOUTI M.A., ALLEN S.J., AHMAD M.N., 2005A, *Effect of OH and silanol groups in the removal of dyes from aqueous solution using diatomite*, Water Res. 39, 922–932.

KHRAISHEH M.A.M., AL-GHOUTI M.S., 2005B, *Enhanced dye adsorption by microemulsion-modified calcined diatomite (μE-CD)*, Adsorpt. 11, 547–559.

LEI L.C., DAI Q.Z., ZHOU M.H., ZHANG X.W., 2007, *Decolorization of cationic red X-GRL by wet air oxidation: Performace optimization and degradation mechanism*, Chemosphere. 68, 1135–1142.

LI H.L., LEI H.Y., YU Q., LI Z., FENG X., YANG B.J., 2010, *Effect of low frequency ultrasonic irradiation on the sonoelectro-Fenton degradation of cationic red X-GRL*, Chem. Eng. J. 160, 417–422.

LI Y.H., DU Q.J., LIU T.H., QI Y., ZHANG P., WANG Z.H., XIA Y.Z., 2011, *Preparation of activated carbon from Enteromorpha prolifera and its use on cationic red X-GRL removal*, Appl. Surf. Sci. 257, 10621–10627.

LIM J.L., OKADA M., 2005, *Regeneration of granular activated carbon using ultrasound*, Ultrason. Sonochem. 12, 277–282.

LIN J.X., ZHAN S.L., FANG M.H., QIAN X.Q., 2007, *The adsorption of dyes from aqueous solution using diatomite*, J. Porous Mater. 14, 449–455.

QIU B., CHENG X., SUN D.Z., 2012, *Characteristics of cationic Red X-GRL biosorption by anaerobic activated sludge*, Bioresour. Technol. 113, 102–105.

REN Z.J., GAO H.M., ZHANG H.Q., LIU X., 2014, *Effects of fluxes on the structure and filtration properties of diatomite filter aids*, Int. J. Miner. Process. 130, 28–33.

SAIDI R., TLILI A., FOURATI A., AMMAR N., OUNIS A., JAMOUSSI F., 2012, *Granulometric distribution of natural and flux calcined chert from Ypresian phosphatic series of Gafsa Metlaoui basin compared to diatomite filter aid*, IOP Conf. Ser. Mater. Sci. Eng. 28, 1–8.

SUN Z.M., YANG X.P., ZHANG G.X., ZHENG S.L., FROST R.L., 2013, *A novel method for purification of low grade diatomite powders in centrifugal fields*, Int. J. Miner. Process. 125, 18–26.

TSAI W.T., HSIEN K.J., YANG, J.M., 2004, *Silica adsorbent prepared from spent diatomaceous earth and its application to removal of dye from aqueous solution*, J. Colloid Interface Sci. 275, 428–433.

VIJAYARAGHAVAN K., MAO J., YUN Y.S., 2008, *Biosorption of methylene blue from aqueous solution using free and polysulfone-immobilized Corynebacterium glutamicum: batch and column studies*, Bioresour. Technol. 99, 2864–2871.

WANG H., ZHU M.F., LI Y.G., ZHANG Q.H., WANG H.Z., 2011, *Mechanical properties of dental resin composites by co-filling diatomite and nanosized silica particles*, Mater. Sci. Eng.: C. 31, 600–605.

WU J.S., LIU C.H., CHUB K.H., SUEN S.Y., 2008, *Removal of cationic dye methyl violet 2B from water by cation exchange membranes*, J. Membrane Sci. 309, 239–245.

XIAO W.S., LI Y.C., LIU J., WEN K.N., CHEN J.Y., 2004, *High-pressure and high-temperature phase transformation of cristobalite at a pressure of up to 63 GPa*, Nucl. Technol. 27, 926–930. (in Chinese).

YU H.W., FUGETSU B., 2010, *A novel adsorbent obtained by inserting carbon nanotubes into cavities of diatomite and applications for organic dye elimination from contaminated water*, J. Hazard. Mater. 177, 138–145.